ACS APPLIED NANO MATERIALS

www.acsanm.org Article

Nanocomposite Photoanodes Consisting of p-NiO/n-ZnO Heterojunction and Carbon Quantum Dot Additive for Dye-Sensitized Solar Cells

Tesfaye Abebe Geleta and Toyoko Imae*

Cite This: *ACS Appl. Nano Mater.* 2021, 4, 236–249 Read Online

ACCESS | Metrics & More | Article Recommendations | Supporting Information

ABSTRACT: To increase the performance of power conversion efficiency of dye-sensitized solar cells (DSSCs), in the current paper, nanocomposites of n-type ZnO and p-type NiO semiconductors were constructed as photoanodes in DSSCs. Furthermore, the influence of the addition of carbon quantum dots on the nanocomposites of n-ZnO and p-NiO was evaluated. The efficiency achieved was 1.58 times of that of ZnO with addition of 8 wt % NiO. Moreover, the doping of carbon quantum dots in the nanocomposites of ZnO/NiO(8 wt %) enhanced the efficiency up to 3.8 times of that of ZnO/NiO(8 wt %). The value (13.02% (430 nm LED@100 W/m^2)) was the highest among that of the carbon dot-incorporating DSSCs. NiO and ZnO semiconductors created a p−n heterojunction, gave rise to faster separation of charges, and minimized the recombination of electrons. Carbon quantum dots promoted the charge carrier transport by converting photon to charge and reducing the potential barrier of the charge carrier at the interfaces of n-ZnO/carbon dots and carbon dots/p-NiO. These results suggest that the adequate selection of the band gap energy levels of the materials induces the preferable charge separation. Especially, the effect reducing the potential barrier of charge carriers by carbon quantum dots is prominent to improve the photovoltaic efficiency of the DSSCs. Thus, the nanoscale materials of ZnO, NiO and Cdots were promising for the enhancement of photovoltaic performance.

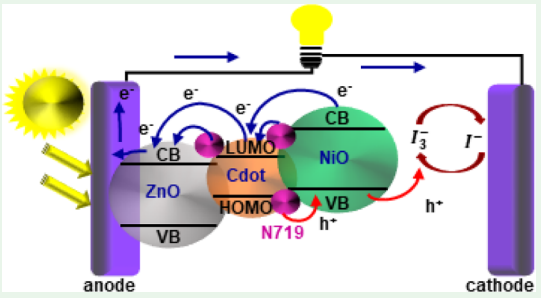

KEYWORDS: *p-NiO/n-ZnO heterojunction, carbon quantum dot, nanocomposite photoanode, power conversion efficiency, dye-sensitized solar cell*

1. INTRODUCTION

Among technologies toward renewable energies, photovoltaics is appealing to the direct transformation of solar energy into electricity. However, the popularized silicon-based photovoltaic cells are adverse in the photovoltaic market owing to their high costs. Conversely, dye-sensitized solar cells (DSSCs) are cost-effective for the reasons of low-cost resources and easy assembly processes. The band gap edge of an ideal DSSC photoanode must fit with a band gap assembly of the sensitizer intended for the competent injection of electrons. The metal oxide materials are mostly used for the construction of photoanodes because of the notable surface area and porous structure being available to the dye adsorption onto the semiconductor.[1] The structure of the photovoltaic cell should afford two principles: the generation of electrons/holes in semiconductor materials by photosensitizing and their transfer to electricity through the conductive contact. The most common DSSCs are composed of the TiO_2 semiconductor and the dye sensitizer.[2] ZnO has high stability against photocorrosion, an adequate band gap (3.37 eV) and an exciton binding energy (60 meV).[3] Thus, ZnO also can be useful for electronic and optoelectronic applications such as light-emitting diodes, photovoltaic devices, and sensor materials. Recently, nanometal oxide semiconductors have drawn abundant attention to photovoltaics and optoelectronics because of their characteristic optical, electrical, and chemical properties.[4]

The significant issue to approve the power conversion efficiency (PCE) of DSSCs is how to raise the efficient separation of charge (electron/hole), delay their recombination, and accelerate the charge carrier transfer across the metal oxide-based semiconductor network. Numerous techniques have been developed to improve the photoanode by facilitating the electron−hole pair separation and their transportation, promoting the longevity of DSSCs, and enhancing their light-harvesting performance.[5,6] The PCEs of DSSCs consisting of the heterojunction (n−n, p−p, or p−n) photoanode/photocathode such as SnO_2/TiO_2 (2.91%),[7] ZnO/ZrS_2 (3.50%),[8]

Received: September 20, 2020
Accepted: December 11, 2020
Published: January 4, 2021

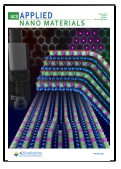

https://dx.doi.org/10.1021/acsanm.0c02547
ACS Appl. Nano Mater. 2021, 4, 236–249

Scheme 1. Scheme of Synthesis of (A) ZnO NPs, (B) NiO NPs, (C) Cdots, and (D) ZnO/NiO/Cdot Nanocomposites

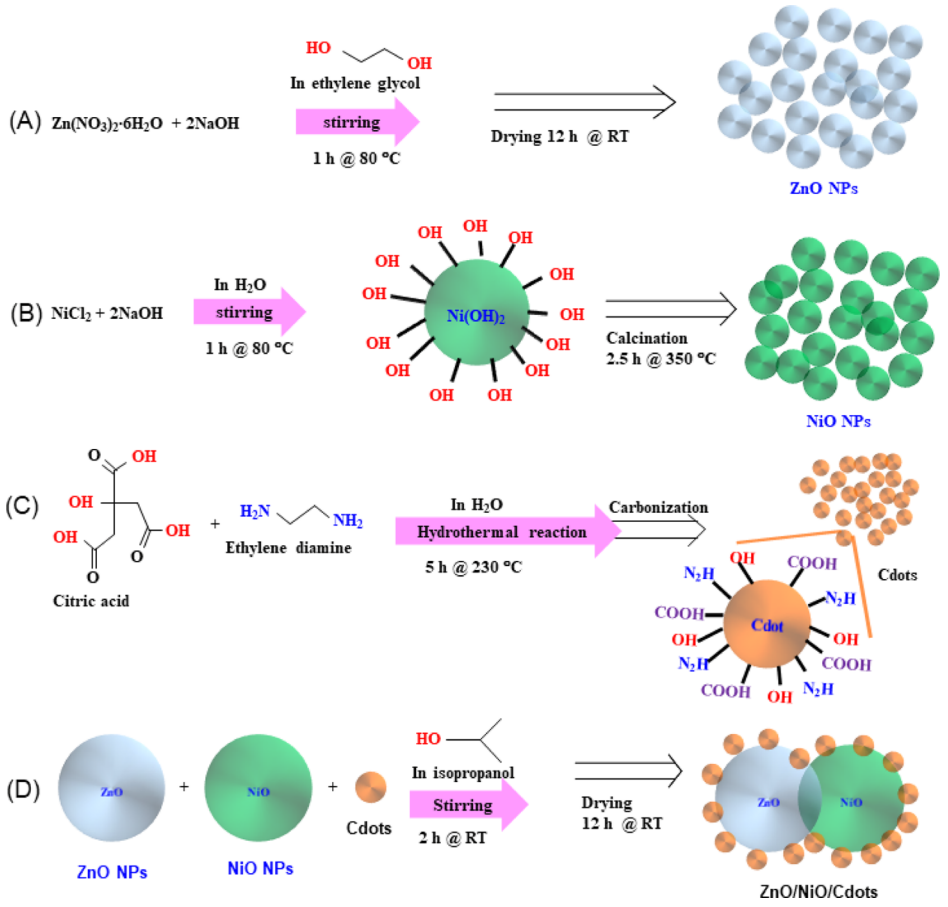

and ZnO/CuO (2.70%)[9] photoanodes and the NiO/CuO (0.50%)[10] photocathode have been reported, but their PCE values were still low. Further modification by doping carbonaceous materials such as graphene or carbon nanotubes (CNTs) has fascinated significant attention because of the uniqueness in their structural and optoelectronic properties, which improves the collection and transport of the charge carrier.[7,11] The performance of the TiO_2/CNT (6.97%) photoanode was enhanced 39% of that of TiO_2 (5.01%)[12] and that of the SnO_2−TiO_2/graphene (3.37%) photoanode was 16% higher than that of SnO_2−TiO_2 (2.91%).[7] Although carbon quantum dots (Cdots) are the nanoscale carbon materials and have similar graphitic structures as other carbonaceous materials, the main advantages of Cdots different from them are easy synthesis,[13] hydrophilicity, inherent conductivity,[14,15] low toxicity,[16] photostability,[17] high surface passivation, excellent biocompatibility,[18] low cost, and environmental friendly.[19] The PCEs of the nanocomposite DSSCs were 5.92% for the ZnO/Cdot electrode[20] and 9.85% for the NiO/Cdot electrode.[21] Thus, the Cdots played a great role as charge carrier transporters to enforce the PCE of the photovoltaic cells.

In this work, we were motivated to further approve the PCE of the photoanode of n-ZnO-based DSSCs by two sequential effects: first, doping the p-NiO semiconductor to form an n-ZnO/p-NiO heterojunction and, second, doping Cdots in the n-ZnO/p-NiO heterojunction to reduce the potential barrier of electron/hole at each boundary of n-ZnO/Cdot and Cdot/p-NiO. Doping of p-NiO will cause fast charge separation and minimize the recombination process because the electric field is generated at the boundary of n-ZnO/p-NiO and the charge carrier is correspondingly driven. Doping of Cdots will give rise to faster charge carrier transport and delay of the direct recombination process. In this research, ZnO and NiO nanoparticles (NPs) with smaller sizes (around 20 nm) are used because the smaller size effectively acts because of the larger surface area.[8] The amine content in Cdots is varied, as it also has effects on the PCE of the DSSC. This research will clarify the roles of the p−n heterojunction and Cdots based on the discussion of the band gaps and the charge transfer mechanisms of the ZnO/NiO/Cdot DSSCs.

2. EXPERIMENTAL SECTION

2.1. Materials and Methods. Nickel chloride ($NiCl_2$, 98%), zinc nitrate hexahydrate ($Zn(NO_3)_2·6H_2O$, 98%), isopropanol (99.5%), ethylene glycol ($(CH_2OH)_2$, 99+%), citric acid anhydrous (CA, 99%), and ethylenediamine (EDA, 99%) were products of Across Organics (USA). N719 (SORALONIX, Germany) was stored in a dark environment. Other reagents were of analytical grade. All reagents were used as received. Indium tin oxide (ITO) glass (11−13 Ω cm^{-2}) was purchased from Aim Core Technology (Taiwan).

Instruments for characterization are a transmission electron microscope (TEM, JEOL ISM-200FX II, Japan, operated at 120 kV), a field-emission gun with a transmission electron microscope (HRTEM, FEI Tecnai G2 F30, Philips, 300 kV), a Fourier transform infrared absorption spectrometer (FTIR, NICOLET 6700, Thermo Scientific, USA), an ultraviolet (UV)−visible absorption spectrometer (JASCO V-670, Japan), a photoluminescence (PL) spectrometer (F-7000, Hitachi High-Technologies Co., Japan), an X-ray diffractometer (XRD, Bruker D2 Phaser, USA), a Brunauer−Emmett−Teller (BET) analyzer (BELSORB Max, Japan), and an X-ray photoelectron

https://dx.doi.org/10.1021/acsanm.0c02547
ACS Appl. Nano Mater. 2021, 4, 236−249

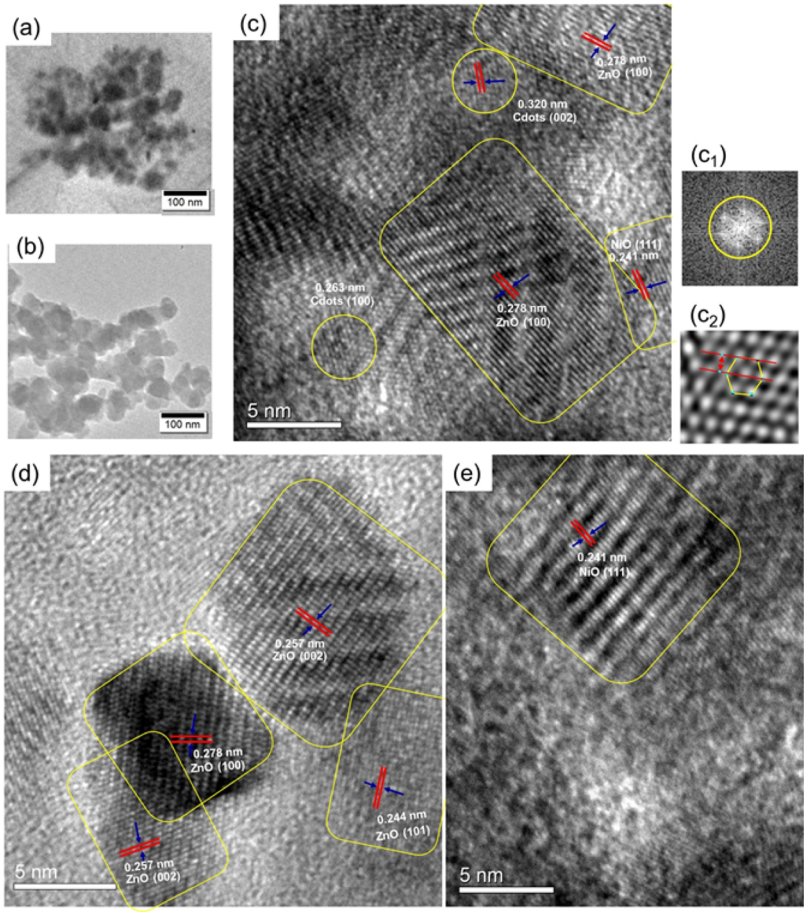

Figure 1. TEM images of (a) ZnO/NiO(8 wt %) and (b) ZnO/NiO(8 wt %)/Cdot(1:1, 5 wt %) and (c)-(e) HRTEM images of ZnO/NiO(8 wt %)/Cdot(1:1, 5 wt %) nanocomposites. (c_1) Fast Fourier transform image and (c_2) inverse fast Fourier transform image of the (100) plane domain of Cdots.

spectrometer (XPS, VG Scientific ESCALAB 250, England). The deconvolution of XPS curves was performed using XPS peak-processing software, where a Lorentzian−Gaussian distribution function and the subtraction of the linear background were applied, and a carbon peak position was used as a reference for the calibration of the XPS spectrum.

2.2. Synthesis of ZnO/NiO/Cdot Nanocomposites. ZnO NPs are the same sample previously prepared and characterized (Scheme 1A).[8] NiO NPs were synthesized using a calcination method.[22] An aqueous NaOH (0.4 M) solution was dropwise added to an aqueous $NiCl_2$ (0.2 M) solution with constant stirring and stirred for 1 h at 80 °C. The precipitates formed were collected by centrifugation (6000 rpm, 10 min) and washed with water, ethanol, and again water. The black NiO NPs were produced by calcining the dried solid for 2.5 h at 350 °C (Scheme 1B). The dispersions of ZnO NPs and NiO NPs (2, 4, 6, 8, and 10 wt %) in isopropanol were stirred for 2 h at room temperature (~25 °C) after sonication for 30 min. Following the same process for ZnO NPs, solids of ZnO/NiO were washed and dried.

Cdots were synthesized based on the bottom-up hydrothermal procedure (Scheme 1C).[23] In short, CA (1.00 g) and EDA in water (10 mL) were heated in a poly(tetrafluoroethylene) (Teflon)-lined autoclave at 230 °C for 5 h. The transparent dark-brown products at CA/EDA = 1:0.5, 1:1, 1:1.5, and 1:2 mole ratios were obtained from the amount of EDA of 167, 335, 502, and 669 μL, respectively. After the dispersion of ZnO/NiO(8 wt %) and Cdots in isopropanol was sonicated for 30 min, it was stirred at room temperature (25 °C) for 2 h. The precipitates (ZnO/NiO(8 wt %)/Cdot) were washed and dried following the procedure for ZnO (Scheme 1D). Nanocomposites at a fixed ZnO/NiO(8 wt %) were prepared at different CA/EDA mole ratios along with amounts of Cdots.

2.3. Fabrication of Solar Cells and Photovoltaic Measurements. Solar cell systems were prepared as previously reported.[8] ITO glass (2 cm × 2 cm) was treated by washing with solvents in a sonicator and exposing to UV−ozone. The ZnO (200 mg) slurry in isopropanol (1 mL) was deposited on an ITO substrate (1 cm × 1 cm) and annealed at 400 °C for 40 min. In a newly prepared ethanol solution of N719 (0.5 mM, 5 mL), the dried ITO/ZnO photoanode was soaked overnight, washed out with water and ethanol and dried at room temperature (~25 °C). The working electrodes of ITO/ZnO/NiO/N719 and ITO/ZnO/NiO/Cdot/N719 photoanodes, the counter electrode of the Pt-deposited ITO glass and solar cells were prepared following the previous report.[8]

The current density−voltage (J−V) curves and other electrochemical parameters were measured on a photo-electrochemical workstation (ZHNAER CIMPS-X, Germany) with a light-emitting diode (LED) light (blue light, λ: 430 nm, 100 W/m^2) and analyzed with THALES software from ZHNAER (XPot 26356, Germany). The calculation of PCE was performed based on eq 1

$$\text{PCE}\ (\%) = \frac{J_{sc} \cdot V_{oc} \cdot \text{FF}}{E} \cdot 100 \qquad (1)$$

where V_{oc}, J_{sc}, FF, and E are the open-circuit voltage, the short-circuit current density, the fill factor, and the incident light intensity (100 W/m^2), respectively. The measurements for minimum two sets of cells were performed five times and averaged. The electrochemical impedance spectroscopy (EIS) data were obtained similarly to the previous report,[8] using an open-circuit voltage (an alternating current (AC) amplitude of 10 mV) in a frequency in the 1 Hz to 10^6 Hz range

https://dx.doi.org/10.1021/acsanm.0c02547
ACS Appl. Nano Mater. 2021, 4, 236−249

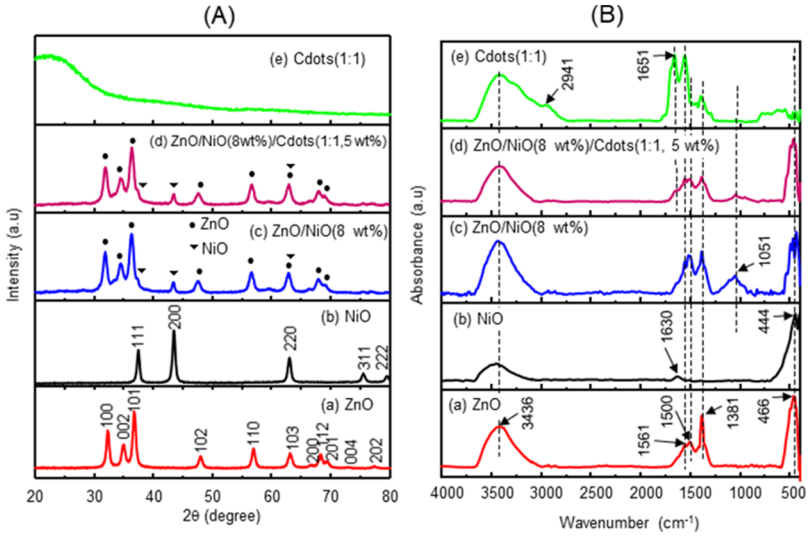

Figure 2. (A) XRD and (B) FTIR spectra of (a) ZnO, (b) NiO, (c) ZnO/NiO(8 wt %), (d) ZnO/NiO(8 wt %)/Cdot(1:1, 5 wt %), and (e) Cdot(1:1) NPs.

under the dark conditions. Intensity-modulated photocurrent spectroscopy (IMPS) and the intensity-modulated photovoltage spectroscopy (IMVS) were performed with a frequency response analyzer, which can deliver both direct current (DC) (light intensities from 30 to 150 W/m^2) and AC components of the illumination by setting the frequency interval from 100 mHz to 10 kHz.

2.4. Determination of Adsorption Amounts of Dye on Electrodes. Adsorption amounts of dye on ZnO/NiO(8 wt %) electrodes loaded with different contents of Cdot(1:1) were determined by immersing the relevant electrodes in a newly prepared ethanol solution of N719 (0.5 mM, 5 mL) overnight, rinsing with water and ethanol, and drying at room temperature (25 °C). Then, the electrodes were kept in an aqueous NaOH solution (1 M, 5 mL) for 12 h to remove the dye adsorbed on the photoanodes. The amounts of the dye in the extracts were evaluated using calibration curves through calorimetry (UV−visible absorption spectrometer, JASCO V-670, Japan), in which absorbance at a 309 nm band of N719 was utilized. Once the concentration of the desorbed dye is known, the loaded mass of dye can be calculated using a mass molarity calculator. Finally, the loaded dye was expressed as weight per weight of the electrode material.

3. RESULTS AND DISCUSSION

3.1. Characterization of Composites. The shape and size of prepared nanocomposites were characterized by TEMimages. As presented in the Supporting Information Figure S1, nanograins of ZnO and NiO had mean sizes of 19.3 ± 3.5 and 21.2 ± 4.3 nm, respectively, which were similar to previously reported values.[8,20,21] However, a TEM image of ZnO/NiO(8 wt %) displayed larger nanograins, where small nanograins of 20 nm size were agglomerated (Figure 1a). The results indicate that when ZnO and NiO(8 wt %) with similar sizes are mixed, they interact attractively, suggesting the possible formation of a heterojunction between them. Moreover, the addition of Cdots on ZnO/NiO(8 wt %) seems to promote the cohesion between ZnO and NiO NPs along of the interposition of Cdots. Thus, the independent 20 nm grains are difficult to see in Figure 1a,b.

Figure 2A shows XRD patterns provided from ZnO, NiO, ZnO/NiO(8 wt %), ZnO/NiO(8 wt %)/Cdot(1:1, 5 wt %), and Cdot(1:1) NPs. There are distinguishable peaks at 2θ angles of 32.22°, 34.93°, and 36.76°. Based on PDF no. 79−1827, these peaks are attributed to the diffractions of (100), (002), and (101) lattice indexes, respectively, of ZnO with a hexagonal wurtzite arrangement.[8] The peaks at 2θ = 37.51°, 43.54°, 63.13°, 75.64°, and 79.61° are referred to NiO with a cubic structure and can be assigned to the planes of (111), (200), (220), (311), and (222), respectively,[24] which are indexed in PDF no. 01−1239. In the nanocomposites of both ZnO/NiO(8 wt %) and ZnO/NiO(8 wt %)/Cdot(1:1, 5 wt %), besides the main Bragg peaks of ZnO, weak peaks are realized at 2θ angles of 37.41°, 43.43°, and 62.96° corresponding to (111), (200), and (220) lattice indexes of NiO, respectively.[4,25,26] It can be referred from these results that NiO(8 wt %) is contained in composites[21] but does not influence crystallographically ZnO, being consistent with the observation of fringes from ZnO and NiO in TEM images. However, there is a report that the XRD peaks have shifted after doping Ni into ZnO because of the distortions in the ZnO host lattice after doping Ni along of different ionic radii of Zn^{2+} (0.74 Å) and Ni^{2+} (0.69 Å).[27] On the present ZnO/NiO(8 wt %) composites, the d-spacings of (100), (002), and (101) planes for ZnO and ZnO/NiO(8 wt %) were 0.277 and 0.281 nm, 0.256 and 0.260 nm, and 0.244 and 0.247 nm, respectively (Figure S2). Thus, the changes of 0.003−0.004 nm in the d-spacings may be judged to have no significant meaning. On the XRD pattern of ZnO/NiO(8 wt %)/Cdot-(1:1, 5 wt %), even if Cdots were doped in ZnO/NiO(8 wt %), the new Bragg peaks were not observed because of the small size of the Cdots with ∼2.5 nm diameter,[21] which is reflected as a broad hump centered around 2θ = ∼22.5° (as shown in Figure 2Ae).[28] The crystallite size (D [nm]) can be evaluated using a formula of Debye−Scherrer[29]

$$D = k\lambda/\beta \cos\theta \quad (2)$$

where k (=0.94) is a Scherrer constant, which depends on the particle shape, λ (=0.1542 nm) is an incident wavelength of the Cu Kα radiation, β [radian] is a full width at half maximum (fwhm) of the selected diffraction peak, and θ [°] is Bragg's diffraction angle obtained as a 2θ value of the relevant index. Thus, the averaged values of crystallinity sizes of ZnO and NiO calculated from the Bragg peaks (nine peaks for ZnO and five peaks for NiO) at 30−80° were 14.3 and 13.9 nm, respectively.

https://dx.doi.org/10.1021/acsanm.0c02547
ACS Appl. Nano Mater. 2021, 4, 236−249

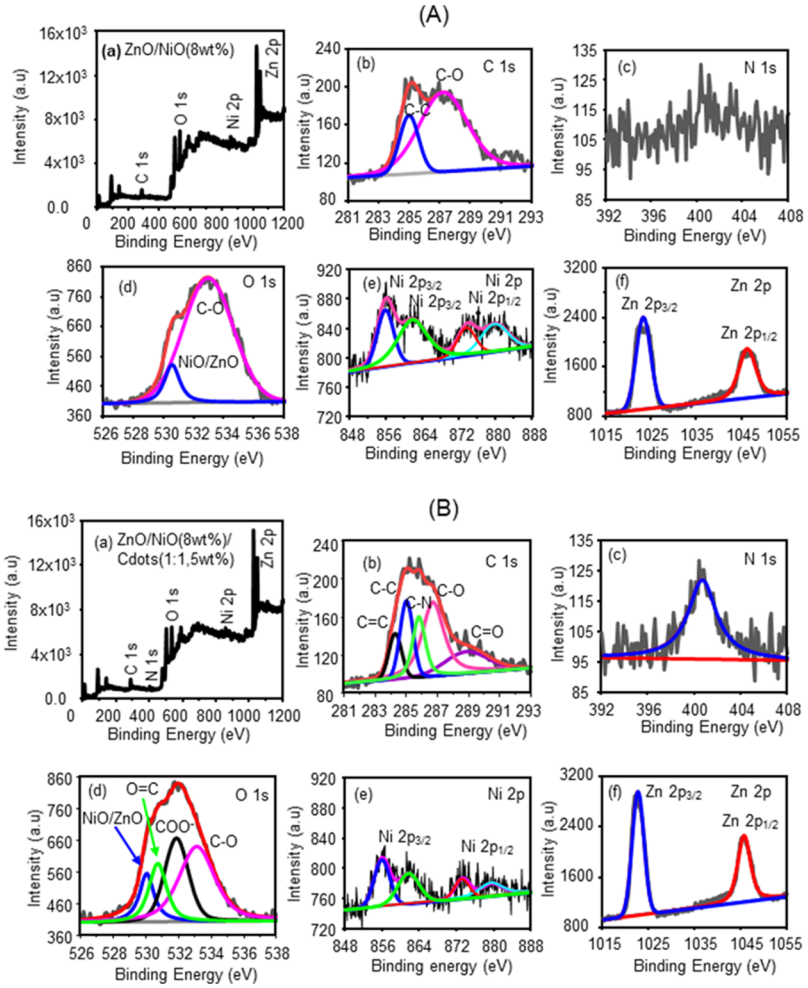

Figure 3. XPS spectra of (A) ZnO/NiO(8 wt %) and (B) ZnO/NiO(8 wt %)/Cdot(1:1, 5 wt %). (a) Full survey spectrum and fine and deconvoluted spectra of (b) C 1s, (c) N 1s, (d) O 1s, (e) Ni 2p, and (f) Zn 2p.

Table 1. Binding Energies and Area Intensities from XPS of ZnO/NiO(8 wt %) and ZnO/NiO(8 wt %)/Cdot(1:1, 5 wt %)

	Zn/NiO(8 wt %)		ZnO/NiO(8 wt %)/Cdot(1:1, 5 wt %)		
element	binding energy (eV)	area intensity (a.u.)	binding energy (eV)	area intensity (a.u.)	assignment
C 1s			284.3	49.8	C═C (aromatic)
	284.9	98.5	285.0	84.9	C−C (ethylene glycol, citric acid)
			285.8	81.1	C−N (amine)
	287.2	361.4	286.7	183.6	C−OH (ethylene glycol, hydroxyl)
			288.8	77.6	C═O (carboxylic)
N 1s			400.7	121.8	N−C (amine)
O 1s	530.5	228.4	530.1	256.8	O−Zn/O−Ni (ZnO/NiO)
			530.8	336.6	O═C (carboxylic)
			531.9	541.3	COO^- (hydroxyl)
	532.9	1722.7	533.1	799.7	C−OH (ethylene glycol)
Ni $2p_{3/2}$	855.8	374.3	855.9	267.9	Ni^{2+} (NiO)
	861.7	630.6	861.6	248.6	Ni^{2+} (NiO)-satellite
Ni $2p_{1/2}$	873.7	181.9	873.2	101.8	Ni^{2+} (NiO)
	879.8	265.7	879.5	140.8	Ni^{2+} (NiO)-satellite
Zn $2p_{3/2}$	1023.2	5999.6	1022.6	6267.9	Zn^{2+} (ZnO)
Zn $2p_{1/2}$	1046.2	4473.6	1045.6	4493.1	Zn^{2+} (ZnO)

These sizes were slightly smaller than those from TEM reported above.

To clarify the coexistence of component crystals, the HRTEM images of the ZnO/NiO(8 wt %)/Cdot(1:1, 5 wt %) nanocomposite were observed because the images can provide the different lattice fringes of different spacings from different nanomaterials. As seen in Figure 1c−e, the majority was the spacing of 0.278 nm assignable to the (100) lattice plane of ZnO[30] and, additionally, the spacings at 0.257, 0.244, and 241 nm, respectively, were of (002) and (101) lattice

https://dx.doi.org/10.1021/acsanm.0c02547
ACS Appl. Nano Mater. 2021, 4, 236−249

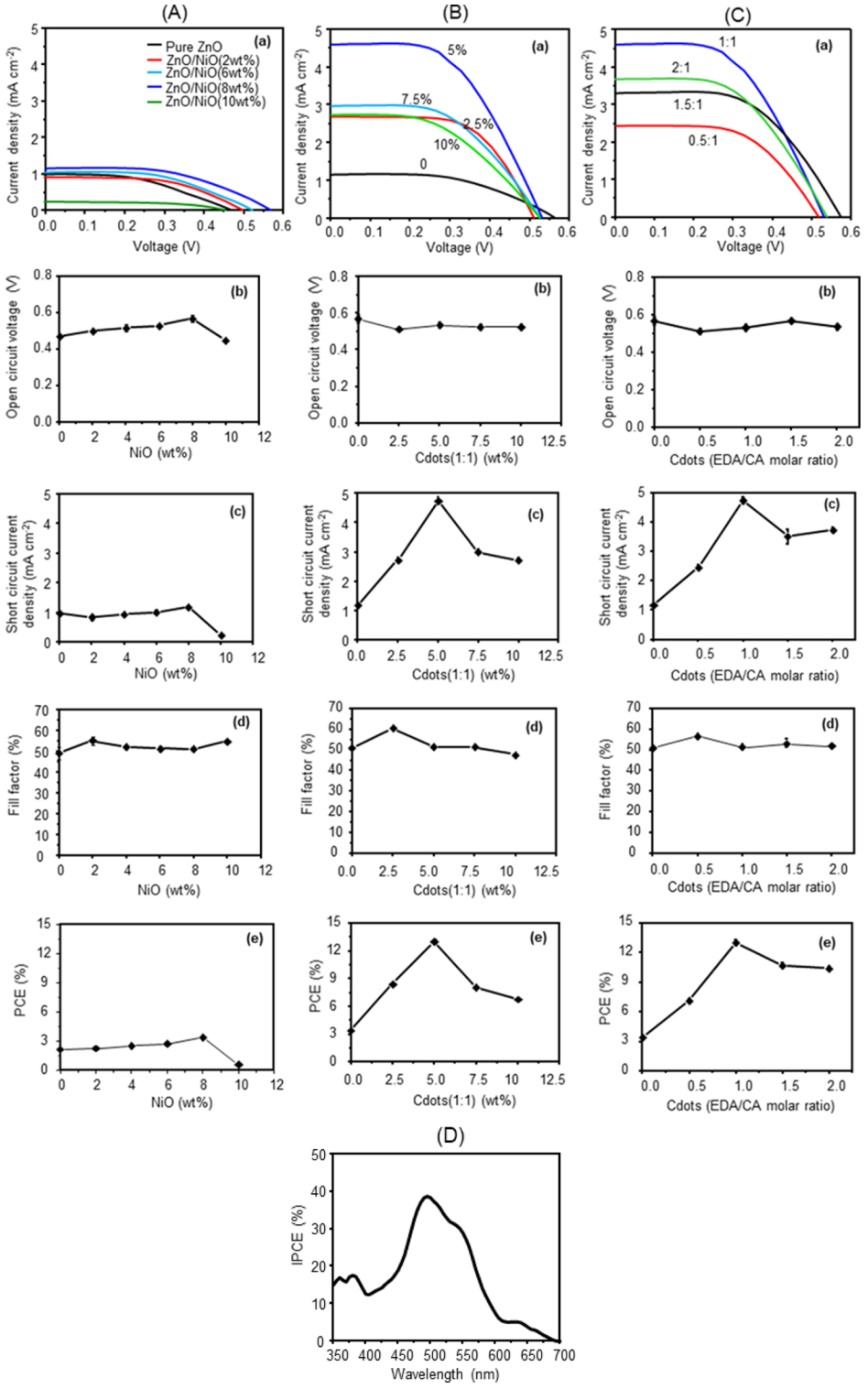

Figure 4. *J*−*V* curves and plots of parameters of (A) ZnO/NiO at various amounts of NiO, (B) ZnO/NiO(8 wt %)/Cdot(1:1) at different contents of Cdots, and (C) ZnO/NiO(8 wt %)/Cdot(5 wt %) with different EDA/CA mole ratios of Cdots. (a) J−V curve, (b) open-circuit voltage, (c) short-circuit current density, (d) fill factor and (e) PCE. (D) IPCE plot of a ZnO/NiO(8%)/Cdot(1:1, 5 wt %) nanocomposite.

planes of ZnO and of the (111) lattice plane of NiO.[30] Spacings of Cdots were measured at 0.320 and 0.263 nm, which are a (002) lattice index and in-plane (100) spacing of the graphitic structure, respectively.[31] Moreover, the crystal domains of ZnO, NiO, and Cdots exist closely or overlap. Thus, the HRTEM image reveals that the aggregation of component nanomaterials in a ZnO/NiO(8 wt %)/Cdot(1:1, 5 wt %) nanocomposite is an aggregate consisting of component nanomaterials but does not influence the crystal structure of each component.

Figure 2B shows FTIR absorption spectra of the relevant materials. An O−H stretching mode was observed as a broad band at 3436 cm^{-1} and bands at 1561, 1500, 1381, and 466 cm^{-1} are attributed to the OH bending, CH_2 bending, CH_2

https://dx.doi.org/10.1021/acsanm.0c02547
ACS Appl. Nano Mater. 2021, 4, 236−249

wagging, and Zn−O stretching vibration modes, respectively, in ZnO NPs,[4] where the carbon-including modes come from ethylene glycol (protector of ZnO). The IR bands of NiO NPs appearing at 3460, 1630, and 444 cm^{-1} are assigned to the O−H stretching, O−H bending, and Ni−O stretching vibrations, respectively.[21] The two bands at high wavenumbers are the contributions of the hydroxylation on NiO NPs.[4] The spectrum of ZnO/NiO(8 wt %) NPs demonstrates that the bands originated from ZnO and NiO, except a new band at 1051 cm^{-1} assigned to a stretching vibration of C−O. This band may come from isopropanol that was used as a solvent for preparing the nanocomposite of ZnO and NiO(8 wt %) NPs.[32] IR bands of Cdots at 3436, 2941, 1651, 1554, and 1389 cm^{-1} can be ascribed to O−H, C−H, C═O, N−H/C═C, and C═C vibrations, respectively, which originate from the graphitic structure, carboxylic acid, and amine groups.[14,33] However, an IR spectrum of ZnO/NiO(8 wt %)/Cdot(1:1, 5 wt %) resembled that of ZnO/NiO(8 wt %), but characteristic bands of Cdots were not clearly revealed because of the small amount (5 wt %) of its coexistence.

The full XPS survey scan of ZnO/NiO(8 wt %) and ZnO/NiO(8 wt %)/Cdot(1:1, 5 wt %) in Figure 3 exhibited the characteristic peaks assigned to C 1s, N 1s, O 1s, Ni 2p, and Zn 2p. Chemical species and the composition in particles can be assessed from fine analysis of XPS in Figure 3, and the binding energies and the area intensities of deconvoluted species are recorded in Table 1. On a C 1s peak, ZnO/NiO(8 wt %) displayed two deconvoluted species, which correspond to aliphatic (sp^3) C−C (284.9 eV) and C−OH (287.2 eV) bonds of ethylene glycol adsorbed onto ZnO during the synthesis. Whereas, the binding energies of the relevant species in ZnO/NiO(8 wt %)/Cdot(1:1, 5 wt %) were at 285.0 and 286.7 eV and the peaks from species of Cdots appeared at 284.3 eV (C═C bond), 285.8 eV (C−N bond), and 288.8 eV (C═O bond).[34] Although ZnO/NiO(8 wt %) does not have a nitrogen element, the amine group (C−NH_2 bond) exists in Cdots of ZnO/NiO(8 wt %)/Cdot(1:1, 5 wt %), and it appeared at 400.7 eV. The O 1s peak in ZnO/NiO(8 wt %) can be deconvoluted into two species at 530.5 and 532.9 eV, which occurred from metal−oxygen bonds (Zn−O and Ni−O bonds) and the O−C bond of ethylene glycol on ZnO, respectively. On the other hand, the O 1s in ZnO/NiO(8 wt %)/Cdot(1:1, 5 wt %) was correspondingly at 530.1 and 533.1 eV, and moreover, two new species of binding energy at 530.8 eV (O═C bond) and 531.9 eV (COO^- bond) originated from carboxylic acid/carboxylate because of the existence of Cdots.[35]

Among four peaks in the Ni 2p region of n-ZnO/p-NiO(8 wt %), the main peak of Ni $2p_{3/2}$ and its satellite were detected at 855.8 eV and at 861.7 eV, respectively. A peak at 873.7 eV corresponds to the main peak of Ni $2p_{1/2}$ and a peak at 879.8 eV is its satellite.[6,21] Similarly, the Ni 2p deconvolution peaks in ZnO/NiO(8 wt %)/Cdot(1:1, 5 wt %) were at 855.9 and 861.6 eV and 873.2 and 879.5 eV for $2p_{3/2}$ and $2p_{1/2}$, corresponding to their main and satellite peaks, respectively. For a Zn 2p high-resolution XPS spectrum of ZnO/NiO(8 wt %), a peak at 1023.2 eV is ascribed to Zn $2p_{3/2}$ and an additional peak at 1046.2 eV is ascribed to Zn $2p_{1/2}$.[34−36] The splitting of spin−orbit between Zn $2p_{3/2}$ and Zn $2p_{1/2}$ is 23 eV for both ZnO/NiO(8 wt %) and ZnO/NiO(8 wt %)/Cdot-(1:1, 5 wt %), suggesting that the chemical state of Zn^{2+} is the same in ZnO/NiO(8 wt %) and ZnO/NiO(8 wt %)/Cdot-(1:1, 5 wt %). From the characterization of XPS, it is revealed that the coexistence of the nanocomposites (ZnO, NiO, and Cdots) was successfully confirmed.

3.2. Photovoltaic Performances of Nanocomposite Electrodes. The electrochemical properties of DSSCs with working electrodes of ZnO/NiO/Cdot composites were investigated in comparison with ZnO/Cdot DSSCs[20] and NiO/Cdot DSSCs.[21] The $J-V$ characteristics of ZnO/NiO nanocomposites at the various contents of NiO were analyzed under blue LED light irradiation (Figure 4Aa). The numerical values of $J-V$ characteristic parameters are shown in Table S1 and Figure 4A(b−e). Although the FF values did not visibly vary with mixing of NiO NPs up to 10 wt %, the V_{oc}, J_{sc}, and PCE values gradually increased up to 8 wt % and significantly decreased at 10 wt %. Thus, the PCE increased to 3.41% in 8 wt % of NiO NPs in ZnO NPs, as shown in Table S1.

The improvement in PCE (2.16%) of the ZnO electrode by adding NiO is still not high enough, but in the meantime, Cdots have outstanding optical characteristics and display high PCE-enhancing performance of a photovoltaic cell.[13,37] Figure 4Ba displays $J-V$ curves of a DSSC consisting of the ZnO/NiO(8 wt %) photoanode added with different amounts of Cdot(1:1). The calculated values are shown in Table S1 and Figure 4B(b−e). The current density was improved after the addition of Cdots, although the voltage was not varied. Correspondingly, although the V_{oc} and FF values did not exhibit so abundant deviation against the variation in the amount of Cdots, the J_{sc} values increased remarkably from 1.18 to 4.75 mA cm^{-2} with addition of up to 5 wt % of Cdot(1:1). However, the increased amount of Cdot(1:1) to 10 wt % resulted in the decrease in the current density to 2.71 mA cm^{-2}. As the PCE of DSSCs is in proportion to the current density, the PCE displayed the maximum (13.02%) at 5 wt % of Cdot(1:1). Thus, the PCE increased 3.8 times of that of the ZnO/NiO(8 wt %) electrode with addition of 5 wt % of Cdot(1:1). This enrichment indicates that the Cdots result in higher charge separation as the charge transporter between ZnO and NiO.

The amine content in Cdots may influence the photovoltaic efficiency. Figure 4C and Table S1 depict the $J-V$ characteristics and the obtained parameters of the ZnO/NiO(8 wt %) photoanode added Cdot(5 wt %) at different CA/EDA mole ratios. Alike the variation in contents of Cdots, although the V_{oc} and FF values do not vary much, the J_{sc} values showed the maximum value at 1:1 ratio and, finally, the PCE, affected by these parameters (V_{oc}, FF, and J_{sc}), revealed the highest PCE of 13.02% at Cdot(1:1). The current numerical values were reproducible. For instance, in the performance of ZnO/NiO(8 wt %) and ZnO/NiO(8 wt %)/Cdot(1:1, 5 wt %), measurements done five times for separately prepared cells provided approximately similar values.

Figure 4D displays an incident photon-to-current conversion efficiency (IPCE) spectrum of the ZnO/NiO(8 wt %)/Cdot-(1:1, 5 wt %) nanocomposite. The maximum IPCE value was 38.8% at 495 nm. Then, the IPCE value at a certain wavelength λ can be estimated by following eq 3[21]

$$\text{IPCE}\ (\%) = \frac{J_{sc}\cdot 1240}{P_{in}\cdot\lambda}\cdot 100 \tag{3}$$

where P_{in} is an incident intensity. From eq 3 and the J_{sc} value (4.75 mA/cm^2) in Table S1, obtained at a light source of 430 nm with an incident light intensity of 100 W/m^2, the calculated IPCE value of the ZnO/NiO(8 wt %)/Cdot(1:1, 5 wt %)

https://dx.doi.org/10.1021/acsanm.0c02547
ACS Appl. Nano Mater. 2021, 4, 236−249

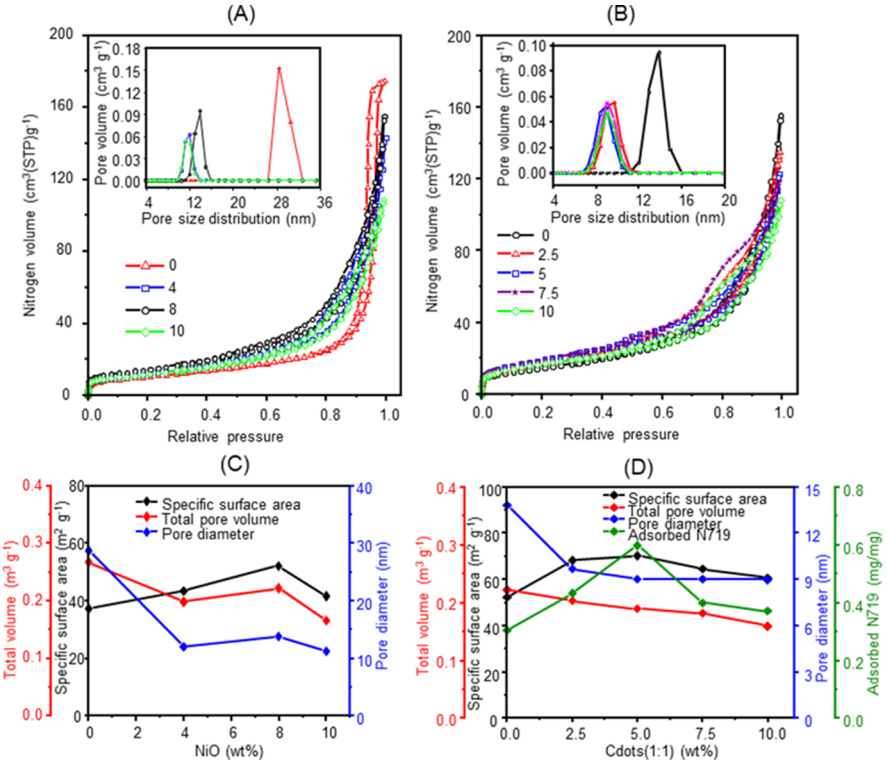

Figure 5. Nitrogen adsorption−desorption isotherms at 77 K and the analyzed parameters of (A,C) ZnO combined with various NiO quantities (0−10 wt %) and (B,D) ZnO/NiO(8 wt %) loaded with different contents (0−10 wt %) of Cdot(1:1). The insets indicate the relevant distribution curves of pore sizes. (D) includes the amount of adsorbed N719.

nanocomposite was 13.7%. This value was almost consistent with the measured IPCE value (15.1%) at 430 nm in Figure 4D.

3.3. Role of Additives (NiO and Cdots) in Photovoltaic Efficiency of ZnO-Based DSSCs. To verify the influence of the additives of NiO and Cdots in ZnO-based DSSCs, some parameters related to surface properties of electrode materials, dye adsorptions, and PL behaviors of Cdots were examined. Nitrogen adsorption−desorption isotherms for the ZnO mixed with different amounts of NiO were measured at 77 K. The isotherms, the distribution curves of pore size, and analyzed parameters are revealed in Figure 5A,C and Table S2. The isotherms of three ZnO/NiO nanocomposites fitted to type II except ZnO of type IV. The highest specific surface area (52.2 $m^2 g^{-1}$) was achieved at 8 wt % of NiO in ZnO and it was about 40% improved than that (37.2 $m^2 g^{-1}$) of ZnO, although the pore diameter and volume tended to decrease with addition of NiO. The surface area varied after NiO was loaded because the variation in the interfacial surface area contacting between the ZnO and NiO NPs changed. The diminution of the average pore volume and diameter may be the mutual overlap of NiO and ZnO NPs in the ZnO/NiO nanocomposites, in concurrence with the aspect of aggregates as observed in the TEM image given above. Further nitrogen adsorption−desorption investigation was performed for nanocomposites of Cdot(1:1) loaded on ZnO/NiO(8 wt %). The results in Figure 5B,D and Table S2 revealed the enhancement of the specific surface area up to 5 wt % Cdot(1:1) and then the decrease in the higher amount (7.5 and 10 wt %) of Cdot(1:1), while the pore volume and pore diameter slightly decreased with loaded Cdots on ZnO/NiO(8 wt %).

Here, the dye (N719) adsorption examination was performed for various amounts of Cdot(1:1) loaded in ZnO/NiO(8 wt %), and the amounts of dye loaded on photoelectrodes are summarized in Table S2 and plotted in Figure 5D. The adsorption of N719 was maximized and then decreased with the increasing amount of Cdot(1:1). It should be focused that the amount of Cdot(1:1) at the maximum dye adsorption is the same as that under the condition of the highest surface area, where the PCE was the highest (see Table S1). The increased specific surface area is raised by the binding of Cdots on the ZnO surface and results in the higher dye adsorption, which yields strongly the enhancement of the PCE of the ZnO/NiO(8 wt %)/Cdot(1:1, 5 wt %) electrode-based DSSC. Similar correlation of the highest specific surface area and the highest PCE also occurred even in the case of NiO loaded on ZnO, where the maximum of both parameters was at 8 wt % NiO. Thus, the surface area may play an important role in adsorbing dye and the high light-harvesting ability, achieving the high enhancement of ZnO/NiO PCE. It can be confirmed that the PCE of the Cdot-loaded electrode is significantly improved by the larger amounts of dye adsorption owing to the achieved wider surface area and by the enlarged light absorbance. Meanwhile, when an excessive amount of Cdot is loaded on ZnO/NiO(8 wt %), overaccumulation of Cdot could occur, leading to the blocking of certain active sites for dye absorption on the surface of ZnO/NiO(8 wt %) and thus the decreased dye adsorption amount.

The PL measurement is available to confirm the effects of the fluorescent material (Cdots) on the nanocomposites of metal oxides (ZnO/NiO(8 wt %)) because the PL intensities of ZnO and NiO are weak (at most 10 wt % of Cdots).[20,21] The PL spectra of different CA/EDA mole ratios of Cdot(5 wt

https://dx.doi.org/10.1021/acsanm.0c02547
ACS Appl. Nano Mater. 2021, 4, 236−249

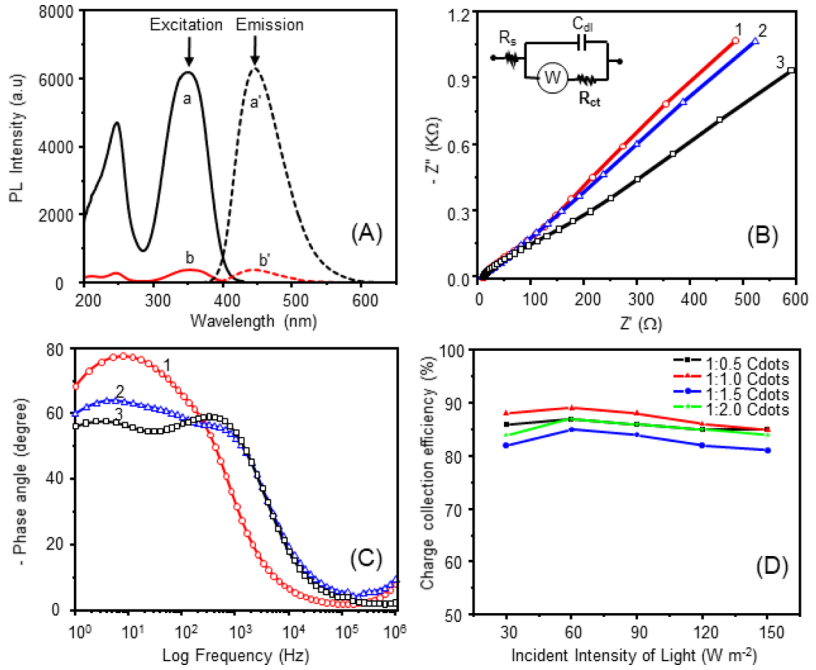

Figure 6. (A) PL excitation (a,b) and emission (a′,b′) spectra of (a,a′) Cdots and (b,b′) ZnO/NiO(8 wt %)/Cdot(1:1, 5 wt %), (B) Nyquist plots and (C) Bode phase curves of EIS of (1) ZnO, (2) ZnO/NiO(8 wt %), and (3) ZnO/NiO(8 wt %)/Cdot(1:1, 5 wt %), and (D) charge collection efficiency calculated from IMPS and IMVS at various light intensities for ZnO/NiO(8 wt %)/Cdot cells at different CA/EDA mole ratios of Cdots. The inset in (B) is the used model circuit.

%) on ZnO/NiO(8 wt %) are shown in comparison with those of Cdots in Figures 6A and S3. Cdot(1:0.5), Cdot(1:1), Cdot(1:1.5), and Cdot(1:2) displayed a strong blue emission band at 446 nm under the excitation at 338, 351, 353, and 355 nm, respectively, but Cdot(1:1) resulted in the highest emission intensity. The PL spectra of ZnO/NiO(8 wt %)/Cdot(5 wt %) were remarkably quenched depending on the CA/EDA mole ratio of Cdots: The PL quenching from that of pristine Cdots was 53, 94, 81, and 71% at a CA/EDA of 1.0.5, 1:1, 1:1.5, and 1:2, respectively. It should be especially noticed that the highest quenching (94%) occurred on a ZnO/NiO(8 wt %)/Cdot(1:1, 5 wt %) nanocomposite, which resulted in the highest performance of DSSCs. The result indicates that the photon energy gained by Cdots was consumed by ZnO/NiO(8 wt %), maybe, for enhancing the PCE value.[20]

The charge transfer can be evaluated by EIS performed by applying an open-circuit voltage bias.[8,38,39] The internal and charge transfer resistances (R_s and R_{ct}) were evaluated via fitting the Nyquist plot on a model circuit (Figure 6B). The achieved numerical values for ZnO, ZnO/NiO(8 wt %), and ZnO/NiO(8 wt %)/Cdot(1:1, 5 wt %) electrodes are displayed in Table S3 with the values of PCE. Although the internal resistance did not reveal the significant variation by addition of NiO and Cdots, the charge transfer resistance showed a meaningful variation. Thus, the lowest charge transfer resistance (15.3 Ω) for ZnO/NiO(8 wt %)/Cdot(1:1, 5 wt %) indicates the faster electron transfer in this electrode in connection with the highest PCE.

Beside the charge transfer resistance, the lifetime of an electron (τ_e) in the DSSC is a valuable indicator for evaluating the recombination phenomenon on an electrode. This value is found from a middle peak frequency ($f_{mid} = \omega_{mid}/2\pi$, ω: characteristic angular frequency) in a Bode phase plot (Figure 6C), based on eq 4[8,40]

$$\tau_e = \frac{1}{\omega_{mid}} = \frac{1}{2\pi f_{mid}} \quad (4)$$

Once a middle peak frequency lowers, it implies that the lifetime of an electron becomes longer and the longer lifetime diminishes the rate of recombination for raising the advance of PCE in DSSCs. The lifetimes of an electron calculated from Figure 6C, with the aid of eq 4, were 20.1, 27.9, and 41.9 ms for ZnO, ZnO/NiO(8 wt %), and ZnO/NiO(8 wt %)/Cdot-(1:1, 5 wt %) electrodes, respectively, as listed in Table S3. As a result, the ZnO/NiO(8 wt %)/Cdot(1:1, 5 wt %) electrode attained the longest lifetime of electrons, which provides the high PCE of DSSCs.

The electron transfer time (τ_{tr}) and the charge recombination time (τ_{rec}) in DSSCs are obtainable from IMPS and IMVS, respectively. They are expressed by[39,41,42]

$$\tau_{tr} = \frac{1}{2\pi f_{IMPS}} \quad (5)$$

$$\tau_{rec} = \frac{1}{2\pi f_{IMVS}} \quad (6)$$

where f_{IMPS} and f_{IMVS} are the characteristic frequencies of the minima in IMPS and IMVS imaginary spaces, respectively. The times for electron transport and recombination are plotted, in Figure S4, for the four different CA/EDA mole ratios of Cdots loaded on ZnO/NiO(8 wt %) photoanodes. Both the τ_{tr} and τ_{rec} decreased by intensifying the light because plenty of photoelectrons generated at an incident light of high intensity fill the deep-level traps and resulted in the electron trapping and detrapping with shallower levels.[42] Because the shallow-level traps can capture charges for a short time, if they trap a charge, this charge will be emitted to the nearby bands by the thermal activation process. The photogenerated electrons may

https://dx.doi.org/10.1021/acsanm.0c02547
ACS Appl. Nano Mater. 2021, 4, 236−249

Scheme 2. Energy Level Alignments of (a) Noncontacted n-ZnO/p-NiO, (b) Contacted n-ZnO/p-NiO, and (c) Contacted n-ZnO/Cdot/p-NiO

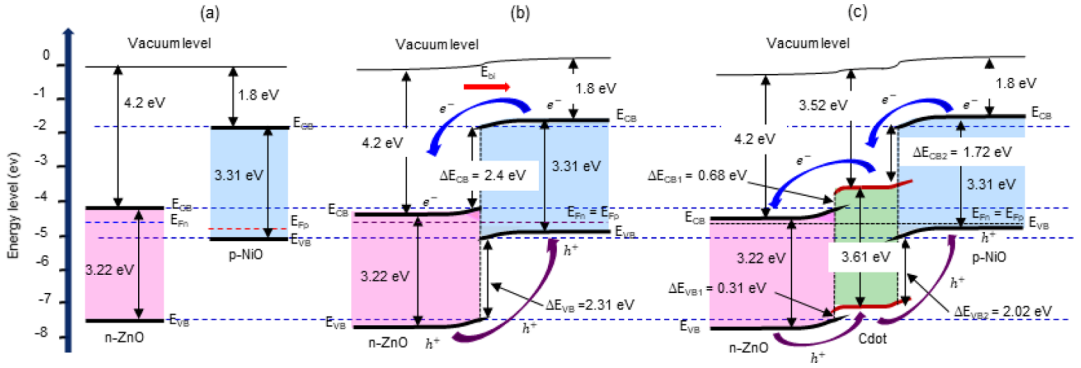

suffer capture and release of the mid-gap state as surface traps offer pathways for nonradiative exciton recombination[43] as they are assumed randomly walking within the films of mesoporous NPs. By the theory of semiconductor physics,[41] once the recombination occurs, the falling of electrons from the conduction band to the valence band shortens the electron lifetime, although if the trap states are larger, the lifetime of electrons is longer. Furthermore, electrons generated by photon transfer the electron from the shallow trap to deep trap (the trapping process) and from the deep trap to shallow trap (the detrapping process).[44]

In addition, the most crucial factor for characterizing the overall performance of DSSCs can be estimated to be charge collection efficiency (C_{ce}), as expressed by[41]

$$C_{ce}\ (\%) = \left(1 - \frac{\tau_{tr}}{\tau_{rec}}\right) \times 100 \tag{7}$$

The charge collection efficiencies calculated from eq 7 for different CA/EDA mole ratios of Cdot(5 wt %) loaded on ZnO/NiO(8 wt %) cells are shown in Figure 6D. Among the different CA/EDA mole ratios of Cdots, Cdot(1:1) achieved the greater charge accumulation efficiency, which confirmed the highest PCE of DSSCs obtained with this material. Moreover, the injection of electrons increased the efficiency of charge collection, resulting in the enhancement of the photocurrent density.

Although the Cdot-enhanced metal oxide DSSC was optimized at 10 wt % Cdots of CA/EDA = 1:2 for n-type ZnO DSSCs[20] and at 12.5 wt % Cdots of CA/EDA = 1:1.5 for p-type NiO DSSCs,[21] it was at 5 wt % Cdots of CA/EDA = 1:1 for ZnO/NiO(8 wt %) DSSCs in the present work. Moreover, it should be noted that the PCE (13.02%) of ZnO/NiO(8 wt %)/Cdot was higher than that (5.92 and 9.85%, respectively) of ZnO/Cdot and NiO/Cdot.[20,21] Such improvement may be attributed to the appearance of a p−n junction at the boundary of ZnO (electron majority carrier) with NiO (hole majority carrier). Here, what we keep in mind is that the n-ZnO/p-NiO heterojunction semiconductors would be arranged based on their respective electron affinity and energy band gap edge values, as shown in Scheme 2a. The conduction band offset of ZnO/NiO for the fabricated cell structure can be calculated according to the Anderson model[45]

$$\Delta E_{CB} = \chi_{ZnO} - \chi_{NiO} = 2.40\ \text{eV} \tag{8}$$

where χ is an affinity of the electron and its value is 4.20 eV for ZnO[46] and 1.80 eV for NiO.[47] Then, the valence band of ZnO/NiO can be calculated as

$$\Delta E_{VB} = E_{gZnO} - E_{gNiO} + \Delta E_{CB} = 2.31\ \text{eV} \tag{9}$$

where E_{gZnO} and $E_{gNiO,}$ respectively, are energy gaps of ZnO (3.22 eV) and NiO (3.31 eV) NPs, and in the current work, the values for individual NP were evaluated from UV−visible absorption spectra. Then, the barriers of the electron and hole, respectively, in the ZnO/NiO interface were 2.40 and 2.31 eV. The respective calculated potential barrier of the electron/hole was lower at the boundary of ZnO and NiO than the band gap of each ZnO and NiO.

The energy level of the boundary of p-NiO and n-ZnO is interpreted as follows. Fundamentally, n-ZnO is an electron-rich semiconductor and p-NiO is a hole-rich semiconductor. When two semiconductors are combined without irradiation of light, the high concentration gradient of the charge carrier happens at the heterojunction boundary, resulting in current diffusing through the heterojunction and charge dissociation (positive donor ion in n-ZnO and negative acceptor ion in p-NiO).[48−50] The carriers (electrons and holes) continue to diffuse all the way for the Fermi energy (E_F) to be equalized in both semiconductors, as shown in Scheme 2b. A built-in electric field is directed from n-ZnO to p-NiO through the junction and then bends a band occurred at the heterojunction boundary. This built-in electric field (E_{bi}) separates charge carriers and reduces their recombination as a consequence. Based on their band gap alignments, once the light is illuminated, electrons transport from the p-side to n-side and holes diffuse from the n-side to p-side because the built-in electric field affects.

Hence, a p−n heterojunction contacting at the boundary of ZnO and NiO would assist in the separation of charges and minimization of the recombination process.[48] Therefore, the PCE (3.41%) of the nanocomposite electrode of ZnO and NiO(8 wt %) was improved 1.58 times of that (2.16%) of the ZnO-based DSSC. However, because the hole mobility was slower than the electron mobility, the higher amount of NiO doped in ZnO was not effective for the enhancement of charge separation.[49] Thus, an excess amount (higher than 8 wt %) of NiO doped in ZnO will result in less charge separation and the higher recombination process.

As the energy levels of Cdots are −7.13 eV (HOMO) and −3.52 eV (LUMO),[51] Cdots are positioned at the midpoint of ZnO and NiO in view of their electron affinity, as shown in Scheme 2c. Following similar ways to eqs 8 and 9, the

https://dx.doi.org/10.1021/acsanm.0c02547
ACS Appl. Nano Mater. 2021, 4, 236−249

conduction and valence bands of ZnO/Cdot and Cdot/NiO were 0.68 and 1.72 eV and 0.31 and 2.02 eV, respectively, in the ZnO/Cdot/NiO composite. Thus, the doped Cdot in ZnO/NiO plays a greater role in reducing the electron/hole barrier at each intersection of ZnO/Cdot and Cdot/NiO. The reduced electron/hole barrier will result in higher charge separation and the passivation of the direct recombination that confirms the enhancement of the PCE of the DSSC.

Cdots are nanosized (~3 nm) NPs containing a graphitic core and functional groups such as carboxyl and amine moieties and exert the luminescent effect.[13] The doping of Cdots in n-ZnO/p-NiO successfully encouraged the significant variation in the specific surface area and the higher adsorption amounts of dye (N719). The increase in photon-harvesting materials is one of the important factors enhancing the PCE of a DSSC. Moreover, the characteristic fluorescence of Cdots was quenched by their doping in the nanocomposites of n-ZnO/p-NiO. Cdots-gained photon energy results in the HOMO−LUMO separation and transfers the generated charge to the closest energy level of n-ZnO/p-NiO without the PL. This process is the efficient charge gain of n-ZnO/p-NiO from Cdots and results in the accelerated charge transfer from Cdots to n-ZnO/p-NiO.[52] Thus, the boosted device performance should be highly contributed by the charge transfer from the coexisting Cdots in the ZnO/NiO nanocomposite photoanode. Additionally, when the Cdots were introduced in the n-ZnO/p-NiO heterojunction, they act as an effective charge transporter by reducing the potential barrier at each interface, as seen in Scheme 2c, in the place of the charge separation and the minimization of charge recombination on the direct p−n junction surface (Scheme 2b). Then, the lower potential barrier induces the faster charge transfer, which inhibits charge recombination and improves current collection, that is, the higher charge collection efficiency results from the faster time of electron transport and longer lifetime of electrons.[53] Meanwhile, the longer electron lifetime is more efficient when the recombination is repressed. In consequence, the PCE of the photoanode was improved 3.8 times of that of the ZnO/NiO(8 wt %) photoanode by doped Cdots. In this work, we have evaluated the effects of two additives, NiO and Cdots, in a ZnO-based DSSC photoanode and could conclude that the Cdot additive was strongly effective compared to the NiO additive in ZnO. Through the present work, the PCE of DSSCs was maximized at 5 wt % Cdot(1:1) and under these conditions, the highest specific surface area, the highest dye absorption, the lowest resistance of charge transfer, and the highest lifetime of electrons were achieved.

Table 2 compares the PCE values of metal oxide semiconductor DSSCs with additives of carbon materials, which have been previously reported.[7,12,20,21,54−60] The addition of carbon materials such as graphene and CNTs enhanced excellently the PCE values of metal oxide-based DSSCs, although these materials are relatively expensive and need rather tender preparation procedures different from those of Cdots. Although the addition of Cdots provides comparable efficiency to that of other carbon materials, the efficiency is higher in the order of ZnO < TiO_2 < NiO. Especially, it should be noteworthy that the n-ZnO/p-NiO/Cdot electrode in the current work has a strikingly high photovoltaic effect.

4. CONCLUSIONS

In this work, photoanodes with a n-ZnO/Cdot/p-NiO heterojunction were applied to improve the photovoltaic efficiency of the DSSCs. The p−n heterojunction constructed at the boundary of n-ZnO with p-NiO assists in the separation of the charge carrier and the reduction in charge recombination, and Cdots doped in n-ZnO/p-NiO minimize the potential barrier of the charge carrier at each interface of n-ZnO/Cdot and Cdot/p-NiO. Thus, Cdots play a greater role in both the photon-to-charge conversion and the fast charge transport to advance the efficiency of the photovoltaic device. In addition, the doping of Cdots on n-ZnO/p-NiO semiconductors revealed the enhancement of the specific surface area and higher amount dye (N719) adsorption. Thus, n-ZnO/Cdot/p-NiO photoanode-based DSSCs achieved a performance (PCE) of 13.02%. It should be noticed that the performance of the photovoltaic p−n junction going through Cdots was more effective than n-ZnO/Cdot (5.92%),[20] n-TiO_2/Cdot (6.90%),[60] and p-NiO/Cdot (9.85%)[21] nanocomposites. Thus, it could be confirmed that Cdots influence the n−p type heterojunction photoanode and both n-type and p-type semiconductor photoelectrode-based DSSCs to promise the enhancement of the photovoltaic devices, not only DSSCs but also other devices. To conclude, this study proves that the adequate nanocomposites of the photoelectrodes can be constructed by the suitable band gap alignment and they are highly recommended for enhancing the performance of the photovoltaic device. Then, Cdots are preferable candidates of the constituted heterojunction.

Table 2. Comparison of Photovoltaic Efficiency of the DSSCs on Nanocomposites with Carbon Materials as Additives

electrode	additive	PCE (%)	refse
TiO_2	thermally threated carbon black	5.65	54
TiO_2	CNTs	6.97	12
TiO_2	functionalized graphene	8.13	55
TiO_2	multi-walled CNT	9.05	56
TiO_2	activated single-walled CNT	2.16	57
TiO_2	graphene	8.07	58
TiO_2	nitrogen-doped carbon quantum dot	8.02	59
TiO_2	carbon quantum dot	6.90	60
ZnO	carbon quantum dot	5.92	20
SnO_2/TiO_2	graphene	3.37	7
NiO	carbon quantum dot	9.85	21
ZnO/NiO	carbon quantum dot	13.02	present

Even though our present work has achieved the higher performance of photovoltaic DSSCs compared to previous reports based on the addition of Cdots, the device is not yet complete because of the durability of the liquid electrolyte and dye and, moreover, PCE is still lower than that of perovskite solar cells,[61,62] although the perovskite solar cells have issues of long-term, thermal, and moisture stabilities to be progressed.[63] Therefore, toward the practical applications, our future prospects will be the fabrication of a stable solid electrolyte or a solid hole transport material and a stable photosensitizing dye.[64,65]

■ ASSOCIATED CONTENT

Supporting Information

The Supporting Information is available free of charge at https://pubs.acs.org/doi/10.1021/acsanm.0c02547.

TEM images and particle size distribution of ZnO and NiO, amplified XRD of ZnO and ZnO/NiO(8 wt %) NPs, PL spectra of Cdot(1:1) and ZnO/NiO(8 wt

https://dx.doi.org/10.1021/acsanm.0c02547
ACS Appl. Nano Mater. 2021, 4, 236−249

%)/Cdot(5 wt %), electron transport time measured by IMPS and electron recombination time measured by IMVS for ZnO/NiO(8 wt %)/Cdot(5 wt %) cells, parameters from J−V curves of ZnO/NiO and ZnO/NiO(8 wt %)/Cdot photoanodes, surface properties and amount of N719 adsorption of ZnO/NiO NPs and ZnO/NiO(8 wt %)/Cdot(1:1), and EIS parameters and PCE values for different photoanodes (PDF)

AUTHOR INFORMATION

Corresponding Author

Toyoko Imae − *Graduate Institute of Applied Science and Technology, National Taiwan University of Science and Technology, Taipei 10607, Taiwan; Department of Chemical Engineering and Department of Materials Science and Engineering, National Taiwan University of Science and Technology, Taipei 10607, Taiwan;* orcid.org/0000-0003-2731-1960; Phone: +886 227303627; Email: imae@mail.ntust.edu.tw

Author

Tesfaye Abebe Geleta − *Graduate Institute of Applied Science and Technology, National Taiwan University of Science and Technology, Taipei 10607, Taiwan*

Complete contact information is available at: https://pubs.acs.org/10.1021/acsanm.0c02547

Notes

The authors declare no competing financial interest.

ACKNOWLEDGMENTS

This research was partially supported by the Ministry of Science and Technology, Taiwan (MOST 108-2221-E-011-105-). TAD was financially supported by the National Taiwan University of Science and Technology, Taiwan, for a student scholarship. We thank Prof. B. J. Hwang in the National Taiwan University of Science and Technology, Taiwan, for his kindness for allowing the use of an IPCE instrument. We thank F. J. Rahmania in the National Taiwan University of Science and Technology, Taiwan, for her kind technical assistance in TEM measurements.

REFERENCES

(1) Xin, X.; He, M.; Han, W.; Jung, J.; Lin, Z. Low-Cost Copper Zinc Tin Sulfide Counter Electrodes for High Efficiency Dye-Sensitized Solar Cells. *Angew. Chem., Int. Ed.* **2011**, *50*, 11739−11742.

(2) Gong, J.; Sumathy, K.; Qiao, Q.; Zhou, Z. Review on Dye-Sensitized Solar Cells (DSSCs): Advanced Techniques and Research Trends. *Renewable Sustainable Energy Rev.* **2017**, *68*, 234−246.

(3) Krishnakumar, B.; Imae, T.; Miras, J.; Esquena, J. Synthesis and AZO Dye Photodegradation Activity of ZrS2−ZnO Nano-Composites. *Sep. Purif. Technol.* **2014**, *132*, 281−288.

(4) Nada, A. A.; Selim, H.; Bechelany, M.; El-Sayed, M.; Hegazey, R.; Souaya, E. R.; Kotkata, M. A Novel Photoelectrode of NiO@ZnO Nanocomposite Prepared by Pechini Method Coupled with PLD for Efficiency Enhancement in DSSCs. *Mater. Sci.-Pol.* **2018**, *36*, 327−336.

(5) Mathew, S.; Yella, A.; Gao, P.; Humphry-Baker, R.; Curchod, B. F.; Ashari-Astani, N.; Tavernelli, I.; Rothlisberger, U.; Nazeeruddin, M. K.; Grätzel, M. Dye-Sensitized Solar Cells with 13% Efficiency Achieved Through the Molecular Engineering of Porphyrin Sensitizers. *Nat. Chem.* **2014**, *6*, 242−249.

(6) Zhou, X.; Yang, J.; Cheng, J.; Qiang, Y.; Shi, H.; Xie, Y. High-Efficiency ZnO/NiO Composite Photoanodes with $Zn(Ac)_2$ Ethanol Solution-Processed for Dye-Sensitized Solar Cells. *J. Alloys Compd.* **2018**, *765*, 287−298.

(7) Basu, K.; Selopal, G. S.; Mohammadnezad, M.; Akilimali, R.; Wang, Z. M.; Zhao, H.; Vetrone, F.; Rosei, F. Hybrid Graphene/Metal Oxide Anodes for Efficient and Stable Dye Sensitized Solar Cell. *Electrochim. Acta* **2020**, *349*, 136409−136418.

(8) Geleta, T. A.; Imae, T. Influence of Additives on Zinc Oxide-Based Dye Sensitized Solar Cells. *Bull. Chem. Soc. Jpn.* **2020**, *93*, 611−620.

(9) Abraham, N.; Rufus, A.; Unni, C.; Philip, D. Dye Sensitized Solar Cells Using Catalytically Active CuO-ZnO Nanocomposite Synthesized by Single Step Method. *Spectrochim. Acta, Part A* **2018**, *200*, 116−126.

(10) Tan, R.; Wei, Z.; Liang, J.; Lv, Z.; Chen, B.; Qu, J.; Yan, W.; Ma, J. Enhanced Open-Circuit Photovoltage and Charge Collection Realized in Pearl-Like NiO/CuO Composite Nanowires Based p-Type Dye Sensitized Solar Cells. *Mater. Res. Bull.* **2019**, *116*, 131−136.

(11) Durantini, J.; Boix, P. P.; Gervaldo, M.; Morales, G. M.; Otero, L.; Bisquert, J.; Barea, E. M. Photocurrent Enhancement in Dye-Sensitized Photovoltaic Devices with Titania−Graphene Composite Electrodes. *J. Electroanal. Chem.* **2012**, *683*, 43−46.

(12) Yang, N.; Zhai, J.; Wang, D.; Chen, Y.; Jiang, L. Two-Dimensional Graphene Bridges Enhanced Photoinduced Charge Transport in Dye-Sensitized Solar Cells. *ACS Nano* **2010**, *4*, 887−894.

(13) Essner, J. B.; Baker, G. A. The Emerging Roles of Carbon Dots in Solar Photovoltaics: A Critical Review. *Environ. Sci.: Nano* **2017**, *4*, 1216−1263.

(14) Devadas, B.; Imae, T. Effect of Carbon Dots on Conducting Polymers for Energy Storage Applications. *ACS Sustainable Chem. Eng.* **2017**, *6*, 127−134.

(15) Chang, C. C.; Geleta, T. A.; Imae, T. Effect of Carbon Dots on Supercapacitor Performance of Carbon Nanohorn/Conducting Polymer Composites. *Bull. Chem. Soc. Jpn.* **2020**, DOI: 10.1246/bcsj.20200269.

(16) Li, S.; Guo, Z.; Zhang, Y.; Xue, W.; Liu, Z. Blood Compatibility Evaluations of Fluorescent Carbon Dots. *ACS Appl. Mater. Interfaces* **2015**, *7*, 19153−19162.

(17) Liu, Y.; Zhou, L.; Li, Y.; Deng, R.; Zhang, H. Highly Fluorescent Nitrogen-Doped Carbon Dots with Excellent Thermal and Photo Stability Applied as Invisible Ink for Loading Important Information and Anti-Counterfeiting. *Nanoscale* **2017**, *9*, 491−496.

(18) Baker, S. N.; Baker, G. A. Luminescent Carbon Nanodots: Emergent Nanolights. *Angew. Chem., Int. Ed.* **2010**, *49*, 6726−6744.

(19) Semeniuk, M.; Yi, Z.; Poursorkhabi, V.; Tjong, J.; Jaffer, S.; Lu, Z.-H.; Sain, M. Future Perspectives and Review on Organic Carbon Dots in Electronic Applications. *ACS Nano* **2019**, *13*, 6224−6255.

(20) Efa, M. T.; Imae, T. Effects of Carbon Dots on ZnO Nanoparticle-Based Dye-Sensitized Solar Cells. *Electrochim. Acta* **2019**, *303*, 204−210.

(21) Etefa, H. F.; Imae, T.; Yanagida, M. Enhanced Photosensitization by Carbon Dots Co-adsorbing with Dye on p-Type Semiconductor (Nickel Oxide) Solar Cells. *ACS Appl. Mater. Interfaces* **2020**, *12*, 18596−18608.

(22) Varunkumar, K.; Hussain, R.; Hegde, G.; Ethiraj, A. S. Effect of Calcination Temperature on Cu Doped NiO Nanoparticles Prepared via Wet-Chemical Method: Structural, Optical and Morphological Studies. *Mater. Sci. Semicond. Process.* **2017**, *66*, 149−156.

(23) Song, Y.; Zhu, S.; Xiang, S.; Zhao, X.; Zhang, J.; Zhang, H.; Fu, Y.; Yang, B. Investigation into the Fluorescence Quenching Behaviors and Applications of Carbon Dots. *Nanoscale* **2014**, *6*, 4676−4682.

(24) Mishra, S.; Yogi, P.; Saxena, S. K.; Jayabalan, J.; Behera, P.; Sagdeo, P. R.; Kumar, R. Significant Field Emission Enhancement in Ultrathin Nano-Thorn Covered NiO Nano-Petals. *J. Mater. Chem. C* **2017**, *5*, 9611−9618.

(25) Aydoghmish, S. M.; Hassanzadeh-Tabrizi, S. A.; Saffar-Teluri, A. Facile Synthesis and Investigation of NiO−ZnO−Ag Nano-

composites as Efficient Photocatalysts for Degradation of Methylene Blue Dye. *Ceram. Int.* **2019**, *45*, 14934−14942.
(26) Bhatia, P.; Nath, M. Green synthesis of p-NiO/n-ZnO nanocomposites: Excellent Adsorbent for Removal of Congo Red and Efficient Catalyst for Reduction of 4-Nitrophenol Present in Waste Water. *J. Water. Process Eng.* **2020**, *33*, 101017−101030.
(27) Rana, A. K.; Bankar, P.; Kumar, Y.; More, M. A.; Late, D. J.; Shirage, P. M. Synthesis of Ni-Doped ZnO Nanostructures by Low-Temperature Wet Chemical Method and Their Enhanced Field Emission Properties. *RSC Adv.* **2016**, *6*, 104318−104324.
(28) Siddique, A. B.; Pramanick, A. K.; Chatterjee, S.; Ray, M. Amorphous Carbon Dots and Their Remarkable Ability to Detect 2, 4, 6−Trinitrophenol. *Sci. Rep.* **2018**, *8*, 9770−9780.
(29) Bindu, P.; Thomas, S. Estimation of Lattice Strain in ZnO Nanoparticles: X-ray Peak Profile Analysis. *J. Theor. Appl. Phys.* **2014**, *8*, 123−134.
(30) Liu, H.; Zhou, Q.; Zhang, Q.; Hong, C.; Xu, L.; Jin, L.; Chen, W. Synthesis, Characterization and Enhanced Sensing Properties of a NiO/ZnO p−n Junctions Sensor for the SF_6 Decomposition Byproducts SO_2, SO_2F_2, and SOF_2. *Sensors* **2017**, *17*, 913−926.
(31) Wu, Y.; Wei, P.; Pengpumkiat, S.; Schumacher, E. A.; Remcho, V. T. Development of a Carbon Dot (C-Dot)-Linked Immunosorbent Assay for the Detection of Human a-Fetoprotein. *Anal. Chem.* **2015**, *87*, 8510−8516.
(32) Cortés-López, A. J.; Muñoz-Sandoval, E.; López-Urías, F. Oxygenated Surface of Carbon Nanotube Sponges: Electroactivity and Magnetic Studies. *ACS Omega* **2019**, *4*, 18011−18022.
(33) De, B.; Karak, N. A Green and Facile Approach for the Synthesis of Water Soluble Fluorescent Carbon Dots from Banana Juice. *RSC Adv.* **2013**, *3*, 8286−8290.
(34) Efa, M. T.; Imae, T. Hybridization of Carbon-Dots with ZnO Nanoparticles of Different Sizes. *J. Taiwan Inst. Chem. Eng.* **2018**, *92*, 112−117.
(35) Zhu, D.; Shao, Y. NiO/ZnO Nanocomposite as Electrode Material for Supercapacitors. *Int. J. Electrochem. Sci.* **2018**, *13*, 3601−3612.
(36) Tian, H.; Fan, H.; Dong, G.; Ma, L.; Ma, J. NiO/ZnO p−n Heterostructures and their Gas Sensing Properties for Reduced Operating Temperature. *RSC Adv.* **2016**, *6*, 109091−109098.
(37) Cao, L.; Shiral Fernando, K. A.; Liang, W.; Seilkop, A.; Monica Veca, L.; Sun, Y.-P.; Bunker, C. E. Carbon Dots for Energy Conversion Applications. *J. Appl. Phys.* **2019**, *125*, 220903−220915.
(38) Debelo, T. T.; Ujihara, M. Effect of Simultaneous Electrochemical Deposition of Manganese Hydroxide and Polypyrrole on Structure and Capacitive Behavior. *J. Electroanal. Chem.* **2020**, *859*, 113825−113832.
(39) Abate, M. A.; Chang, J.-Y. Boosting the Efficiency of $AgInSe_2$ Quantum Dot Sensitized Solar Cells via Core/Shell/Shell Architecture. *Sol. Energy Mater. Sol. Cells* **2018**, *182*, 37−44.
(40) Abate, M. A.; Dehvari, K.; Chang, J.-Y.; Waki, K. Aqueous Synthesis of Mn-Doped $CuInSe_2$ Quantum Dots to Enhance the Performance of Quantum Dot Sensitized Solar Cells. *Dalton Trans.* **2019**, *48*, 16115−16122.
(41) Wei, A.; Zuo, Z.; Liu, J.; Lin, K.; Zhao, Y. Transport and Interfacial Transfer of Electrons in Dye-Sensitized Solar Cells Based on a TiO_2 Nanoparticle/TiO_2 Nanowire "Double-Layer" Working Electrode. *J. Renewable Sustainable Energy* **2013**, *5*, 033101−033111.
(42) Wang, X.; Wang, Y.-F.; Luo, Q.-P.; Ren, J.-H.; Li, D.-J.; Li, X.-F. Highly Uniform Hierarchical Zn_2SnO_4 Microspheres for the Construction of High Performance Dye-Sensitized Solar Cells. *RSC Adv.* **2017**, *7*, 43403−43409.
(43) Giansante, C.; Infante, I. Surface Traps in Colloidal Quantum Dots: A Combined Experimental and Theoretical Perspective. *J. Phys. Chem. Lett.* **2017**, *8*, 5209−5215.
(44) Guo, H.; Wang, Y.; Li, G.; Liu, J.; Li, Y. The Persistent Energy Transfer of Eu^{2+} and Dy^{3+} and Luminescence Properties of a New Cyan Afterglow Phosphor α-$Ca_3(PO_4)_2$:Eu^{2+}, Dy^{3+}. *RSC Adv.* **2016**, *6*, 101731−101736.
(45) Wang, H.; Zhao, Y.; Wu, C.; Dong, X.; Zhang, B.; Wu, G.; Ma, Y.; Du, G. Ultraviolet Electroluminescence from n-ZnO/NiO/p-GaN Light-Emitting Diode Fabricated by MOCVD. *J. Lumin.* **2015**, *158*, 6−10.
(46) Tyagi, M.; Tomar, M.; Gupta, V. Trap Assisted Space Charge Conduction in p-NiO/n-ZnO Heterojunction Diode. *Mater. Res. Bull.* **2015**, *66*, 123−131.
(47) Irwin, M. D.; Buchholz, D. B.; Hains, A. W.; Chang, R. P. H.; Marks, T. J. p-Type Semiconducting Nickel Oxide as an Efficiency-Enhancing Anode Interfacial Layer in Polymer Bulk-Heterojunction Solar Cells. *Proc. Natl. Acad. Sci. U.S.A.* **2008**, *105*, 2783−2787.
(48) Pansri, S.; Supruangnet, R.; Nakajima, H.; Rattanasuporn, S.; Noothongkaew, S. Band Offset Determination of p-NiO/n-TiO_2 Heterojunctions for Applications in High-Performance UV Photodetectors. *J. Mater. Sci.* **2020**, *55*, 4332−4344.
(49) Praveen, E.; Peter, I. J.; Kumar, A. M.; Ramachandran, K.; Jayakumar, K. Performance of Phototronically Activated Chitosan Electrolyte in Rare-Earth Doped $Bi_2Ti_2O_7$ Nanostructure Based DSSC. *Mater. Lett.* **2020**, *276*, 128202−128206.
(50) Xu, M.; Li, X.; Jin, C.; He, Z.; Zhang, X.; Zhang, Q. Novel and Dual-Mode Strain-Detecting Performance Based on a Layered NiO/ZnO p−n Junction for Flexible Electronics. *J. Mater. Chem. C* **2020**, *8*, 1466−1474.
(51) Barman, M. K.; Mitra, P.; Bera, R.; Das, S.; Pramanik, A.; Parta, A. An Efficient Charge Separation and Photocurrent Generation in the Carbon Dot−Zinc Oxide Nanoparticle Composite. *Nanoscale* **2017**, *9*, 6791−6799.
(52) Guo, Y.; Jin, Z.; Yuan, S.; Zhao, J.-S.; Hao, M.-Y.; Qin, Y.; Fu, L.-M.; Zhang, J.-P.; Ai, X.-C. Effects of Interfacial Energy Level Alignment on Carrier Dynamics and Photovoltaic Performance of Inverted Perovskite Solar Cells. *J. Power Sources* **2020**, *452*, 227845−227853.
(53) Raïssi, M.; Pellegrin, Y.; Lefevre, F.-X.; Boujtita, M.; Rousseau, D.; Berthelot, T.; Odobel, F. Digital Printing of Efficient Dye-Sensitized Solar Cells (DSSCs). *Sol. Energy* **2020**, *199*, 92−99.
(54) Kang, S. H.; Kim, J.-Y.; Kim, Y.-K.; Sung, Y.-E. Effects of the Incorporation of Carbon Powder into Nanostructured TiO_2 Film for Dye-Sensitized Solar Cell. *J. Photochem. Photobiol., A* **2007**, *186*, 234−241.
(55) Chen, T.; Hu, W.; Song, J.; Guai, G. H.; Li, C. M. Interface Functionalization of Photoelectrodes with Graphene for High Performance Dy-Sensitized Solar Cells. *Adv. Funct. Mater.* **2012**, *22*, 5245−5250.
(56) Chan, Y.-F.; Wang, C.-C.; Chen, B.-H.; Chen, C.-Y. Dye-Sensitized TiO_2 Solar Cells Based on Nanocomposite Photoanode Containing Plasma-Modified Multi-Walled Carbon Nanotubes. *Prog. Photovolt: Res. Appl.* **2013**, *21*, 47−57.
(57) Golobostanfard, M. R.; Abdizadeh, H. Influence of Carbon Nanotube Wall Thickness on Performance of Dye Sensitized Solar Cell with Hierarchical Porous Photoanode. *Microporous Mesoporous Mater.* **2014**, *191*, 74−81.
(58) Tsai, C.-H.; Fei, P.-H.; Wu, W.-C. Enhancing the Efficiency and Charge Transport Characteristics of Dye-Sensitized Solar Cells by Adding Graphene Nanosheets to TiO_2 Working Electrodes. *Electrochim. Acta* **2015**, *165*, 356−364.
(59) Riaz, R.; Ali, M.; Maiyalagan, T.; Anjum, A. S.; Lee, S.; Ko, M. J.; Jeong, S. H. Dye-Sensitized Solar Cell (DSSC) Coated with Energy Down Shift Layer of Nitrogen-Doped Carbon Quantum Dots (N-CQDs) for Enhanced Current Density and Stability. *Appl. Surf. Sci.* **2019**, *483*, 425−431.
(60) Bora, A.; Mohan, K.; Dolui, S. K. Carbon Dots as Cosensitizers in Dye-Sensitized Solar Cells and Fluorescence Chemosensors for 2, 4, 6−Trinitrophenol Detection. *Ind. Eng. Chem. Res.* **2019**, *58*, 22771−22778.
(61) Miyasaka, T. Lead Halide Perovskites in Thin Film Photovoltaics: Background and Perspectives. *Bull. Chem. Soc. Jpn.* **2018**, *91*, 1058−1068.
(62) Jeong, M.; Choi, I. W.; Go, E. M.; Cho, Y.; Kim, M.; Lee, B.; Jeong, S.; Jo, Y.; Choi, H. W.; Lee, J.; Bae, J. H.; Kwak, S. K.; Kim, D.

S.; Yang, C. Stable Perovskite Solar Cells with Efficiency Exceeding 24.8% and 0.3-V Voltage Loss. *Science* **2020**, *369*, 1615−1620.
(63) Jena, A. K.; Kulkarni, A.; Miyasaka, T. Halide Perovskite Photovoltaics: Background, Status, and Future Prospects. *Chem. Rev.* **2019**, *119*, 3036−3103.
(64) Chen, H.-W.; Chiang, Y.-D.; Kung, C.-W.; Sakai, N.; Ikegami, M.; Yamauchi, Y.; Wu, K. C.-W.; Miyasaka, T.; Ho, K.-C. Highly Efficient Plastic-Based Quasi-Solid-State Dye-Sensitized Solar Cells with Light-Harvesting Mesoporous Silica Nanoparticles Gel-Electrolyte. *J. Power Sources* **2014**, *245*, 411−417.
(65) Wadsworth, A.; Moser, M.; Marks, A.; Little, M. S.; Gasparini, N.; Brabec, C. J.; Baran, D.; McCulloch, I. Critical Review of the Molecular Design Progress in Non-Fullerene Electron Acceptors Towards Commercially Viable Organic Solar Cells. *Chem. Soc. Rev.* **2019**, *48*, 1596−1625.

https://dx.doi.org/10.1021/acsanm.0c02547
ACS Appl. Nano Mater. 2021, 4, 236−249